npj | Quantum Materials

www.nature.com/npjquantmats

ARTICLE OPEN

Check for updates

Ultrafast strain engineering and coherent structural dynamics from resonantly driven optical phonons in $LaAlO_3$

J. R. Hortensius[1,3]✉, D. Afanasiev[1,3], A. Sasani[2], E. Bousquet[2] and A. D. Caviglia[1]✉

Strain engineering has been extended recently to the picosecond timescales, driving ultrafast metal–insulator phase transitions and the propagation of ultrasonic demagnetization fronts. However, the nonlinear lattice dynamics underpinning interfacial optoelectronic phase switching have not yet been addressed. Here we perform time-resolved all-optical pump-probe experiments to study ultrafast lattice dynamics initiated by impulsive light excitation tuned in resonance with a polar lattice vibration in $LaAlO_3$ single crystals, one of the most widely utilized substrates for oxide electronics. We show that ionic Raman scattering drives coherent rotations of the oxygen octahedra around a high-symmetry crystal axis. By means of DFT calculations we identify the underlying nonlinear phonon–phonon coupling channel. Resonant lattice excitation is also shown to generate longitudinal and transverse acoustic wave packets, enabled by anisotropic optically induced strain. Importantly, shear strain wave packets are found to be generated with high efficiency at the phonon resonance, opening exciting perspectives for ultrafast material control.

npj Quantum Materials (2020)5:95 ; https://doi.org/10.1038/s41535-020-00297-z

INTRODUCTION

Epitaxy can be used to impose misfit strain capable of altering the properties of materials. Notable examples include the enhancement of ferroelectric and ferromagnetic order[1] and even the engineering of artificial multiferroics at room temperature[2]. Whereas static strain engineering is a well-established paradigm[3–5], ultrafast strain engineering has emerged only recently as an effective method to manipulate functional properties of oxides[6,7], control collective excitations[8–11], induce changes in the band topology[12,13], and drive optoelectronic phase switching[14,15]. The generation of strain pulses traditionally relies on opto-acoustic conversion processes either in the functional material itself or in opto-acoustic transducers, often involving electronic excitation[16]. An inherently different approach is to use ultrashort pulses of light that are tuned in resonance with an infrared-active atomic vibration of a substrate, in order to transform the structural and electronic properties of an epitaxial thin film[14]. This mechanism, applied extensively to insulating lanthanum aluminate ($LaAlO_3$) substrates, governs ultrafast metal–insulator transitions[14], ultrasonic magnetic dynamics[17], and sonic lattice waves[18] in various thin films of strongly correlated oxides. However, the nature of the nonlinear lattice dynamics initiated in the substrate material is not yet fully understood. As strain is naturally related to dynamics of the crystal lattice, here we study light-induced ultrafast lattice dynamics directly in an $LaAlO_3$ substrate. We show that impulsive optical excitation at the photon energy tuned in resonance with a polar stretching of the Al–O bonds drives a non-polar rotational mode of oxygen octahedra via ionic Raman scattering[19]. The anisotropic optically induced strain also generates propagating longitudinal (LA) and transverse acoustic (TA) wave packets. Importantly, shear strain wave packets are found to be produced with extraordinary efficiency close to the phonon resonance. These results uncover an hitherto unknown microscopic feature of ultrafast strain engineering that opens wide perspectives for material control via optically tunable strain.

RESULTS AND DISCUSSION

Experiment

We investigate light-induced structural dynamics in $LaAlO_3$, an insulating substrate utilized extensively in oxide electronics for the epitaxy of correlated materials, including high-T_c cuprate superconductors[20], magnetoresistive manganites[21], and nickelates[22]. At room temperature, $LaAlO_3$ exhibits a distorted perovskite structure (rhombohedral space group $R\bar{3}c$, see Fig. 1a). To resonantly drive the lattice vibrations in (001) $LaAlO_3$ single crystals, we use ultrashort pump pulses in the mid-infrared (mid-IR) frequency range. We tune the photon energy of the pump pulses continuously across the closely lying highest-frequency E_u and A_{2u} infrared-active phonon resonances[23,24]. For the schematics of atomic motion corresponding to the E_u and A_{2u} mode, see Fig. 1b and Supplementary Fig. 3, respectively. The energy was tuned in the experimentally accessible range of 70–180 meV (17–41 THz) and allowed us to compare dynamics excited in the optical transparency window (>130 meV) with structural transient dynamics induced by pulses tuned in resonance with the lattice vibrational modes centered at 81 meV. A high efficiency of ionic Raman scattering is anticipated in $LaAlO_3$ as mutual coupling between optical phonon modes exists and even results in a small negative Lyddane–Sachs–Teller splitting between longitudinal and transverse optical modes[25]. The wide bandgap of $LaAlO_3$ (5.6 eV[26]) as well as the absence of electronic in-gap states[27] ensures the purely structural nature of the photo-induced response.

To track the ensuing dynamics of the lattice, time-resolved optical reflectivity and birefringence measurements are performed using near-infrared probe pulses. The two complementary experimental techniques (for details, see "Methods") are schematically illustrated in Fig. 1c. In the first scheme we monitor the transient differential reflectivity ΔR. The structural dynamics initiated by the pump pulse modulate the sample's dielectric function resulting in a perturbation of the refractive index n, which is imprinted on the ΔR signal. In the second scheme we track the transient optical birefringence $\Delta\theta_B$. The phonon modes of $LaAlO_3$

[1]Kavli Institute of Nanoscience, Delft University of Technology, P.O. Box 5046, 2600 GA Delft, The Netherlands. [2]CESAM QMAT Physique Théorique des Matériaux, Université de Liège, B-4000 Sart Tilman, Belgium. [3]These authors contributed equally: J.R. Hortensius, D. Afanasiev. ✉email: j.r.hortensius@tudelft.nl; a.caviglia@tudelft.nl

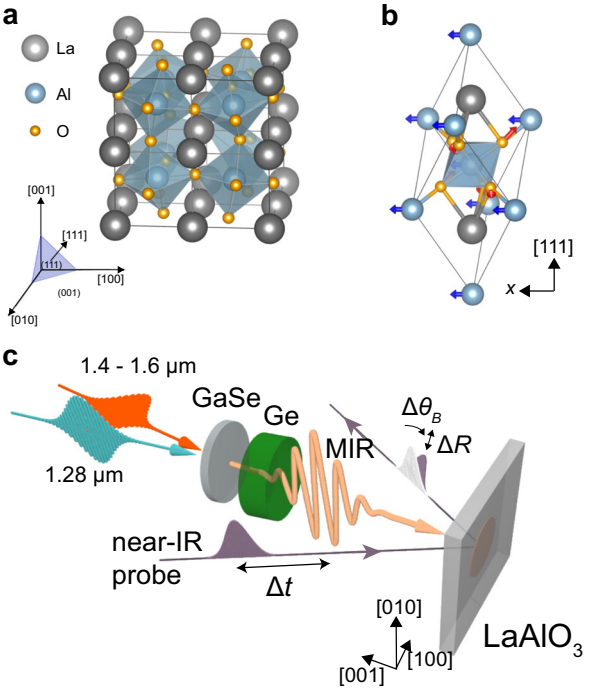

Fig. 1 Crystal structure and experimental geometry. a The crystal structure of $LaAlO_3$, with indications of the different crystallographic directions. The rhombohedral distortion from the high-temperature cubic phase is due to out-of-phase rotations of the oxygen octahedra about the $[111]_{pc}$ axis. **b** Atomic motion corresponding to the infrared-active E_u stretching mode, polarized in the (111) plane in the *x*-direction. **c** Schematic illustration of the experimental scheme. The mid-IR pulse is generated by difference frequency mixing from two near-infrared pulses in a GaSe crystal, after which the mid-IR pulses are filtered by a germanium (Ge) filter. Following the mid-IR excitation, the ensuing changes in optical properties are probed with a time-delayed near-infrared pulse. The pump-induced changes to the reflection intensity ΔR and rotation $\Delta\theta_B$ of the polarization plane are monitored.

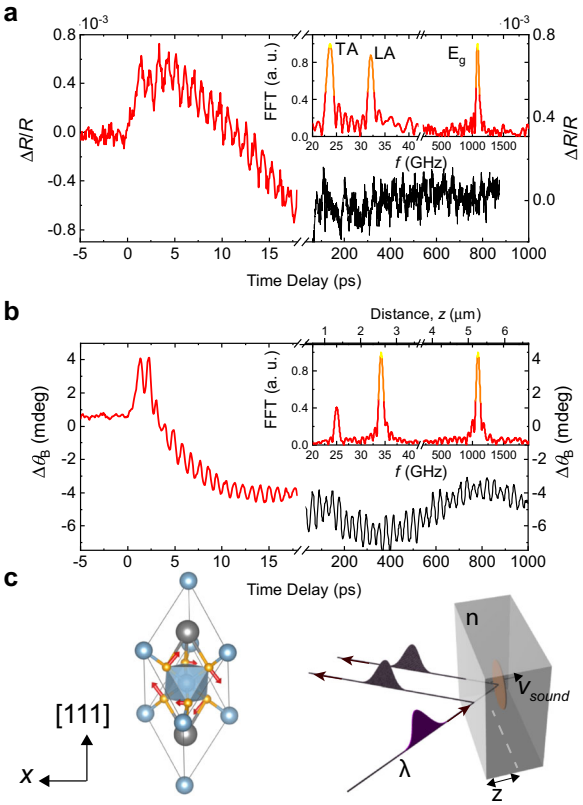

Fig. 2 Photo-induced structural dynamics. Transient changes in the intensity of the reflected probe pulse $\Delta R/R$ (**a**) and the polarization rotation $\Delta\theta_B$ of the probe pulse (**b**) after excitation of the $LaAlO_3$ substrate with a mid-infrared pump pulse of 86 meV (**a**) and 89 meV (**b**) and a fluence of 10 mJ cm^{-2}. The insets show the Fourier spectra of the signals. The top axis in **b** shows the distance *z* which the longitudinal sound wave has propagated at that time. **c** The real-space atomic motion corresponding to the excited E_g mode indicated with arrows (left) and a schematic picture of a strain wave propagating with speed v_{sound} leading to interference between probe light (wavelength λ) reflected at the interface and scattered at the strain wave, depending on the distance *z* which the strain wave has propagated (right).

are intrinsically highly anisotropic, meaning that coherent dynamics of these modes can also modify the off-diagonal components of the permittivity tensor, thereby resulting in a transient birefringence.

Photo-induced structural dynamics

Measurements of transient changes to both the reflectivity and birefringence, using pump pulses at a photon energy tuned in resonance with the infrared-active phonon modes, $h\nu \simeq 85$ meV (21 THz), reveal multiple oscillatory responses at frequencies significantly below the one of the pump (see Fig. 2a, b). The highest-frequency oscillation is centered at 1.1 THz (4.3 meV) and is assigned to the Raman-active E_g soft mode of $LaAlO_3$[24,28] associated with a rhombohedral instability of the $R\bar{3}c$ lattice structure (see Supplementary Note 1). This mode comprises rotations of the oxygen octahedra around an axis perpendicular to the [111] pseudocubic direction as shown in Fig. 2c. The longer time delay further reveals oscillatory components at two discrete frequencies f_{TA} and f_{LA} in the GHz frequency range. Such a pattern originates from interference between light pulses reflected at the crystal surface and reflections from an acoustic wave front propagating into the bulk (Fig. 2c). In transparent materials, the frequency of the oscillations *f* is related to the refractive index *n* of the material at the probe wavelength[27], the speed of sound v_s, the angle θ w.r.t. the sample normal and the wavelength λ of the probe by the relation[29] $f = 2nv_s\cos(\theta)/\lambda$. In our experiments we vary the angle of incidence of the probe beam (the data are not shown here) and find that, while the frequency of the E_g mode remains unchanged, the frequency of the GHz oscillations decreases in agreement with the relation shown above. We extract the corresponding propagation velocities, obtaining $v_{LA} = 6.67$ km s^{-1} and $v_{TA} = 4.87$ km s^{-1}, and find that they match the speed of LA and TA phonons in $LaAlO_3$ propagating in the [001] direction[30]. This acousto-optic conversion is strongly peaked at a phonon wavenumber k_a determined by the probe wavenumber[31], $k_a = 3.2 \times 10^5$ cm^{-1}. Our experiments show that optical excitation with ultrashort resonant mid-IR pulses initiates coherent structural dynamics in both the acoustic and optical branches of the phonon spectrum. Although the optical excitation of a broadband longitudinal acoustic wave front is expected from electrostriction in $LaAlO_3$[32] and/or optical absorption[16], the optical generation of shear strain requires the presence of an equilibrium or light-induced structural anisotropy. We discuss this aspect below, after the analysis of the THz Raman-active mode.

Coherent oxygen octahedra rotations

In our experiments only the lowest-energy Raman-active E_g optical phonon mode was observed. The frequencies of the remaining higher-energy modes (e.g. of A_g symmetry) lie outside

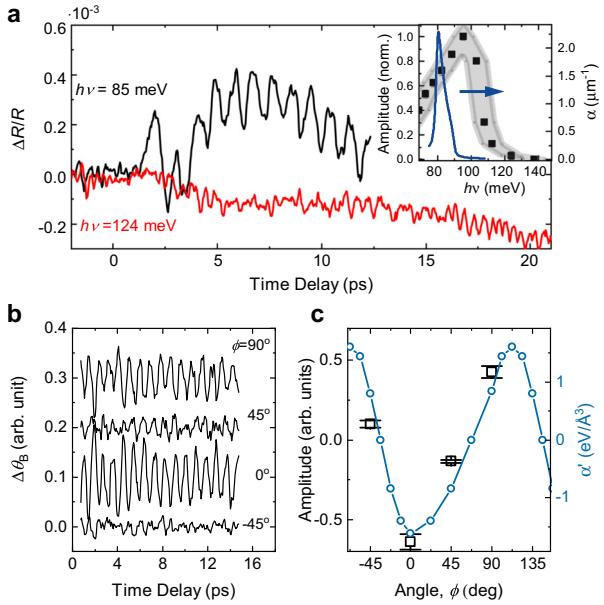

Fig. 3 Light-induced excitation and dynamics of oxygen octahedra rotations. a Time-resolved reflectivity changes of the probe pulse at the central energy of 1.5 eV after mid-IR excitation at photon energies of 83 and 124 meV. Inset: the amplitude of the coherent phonon oscillations at 1.1 THz, as extracted from fitting an exponentially damped sine function to the transient reflectivity changes for different pump photon energies at constant incident fluence. The thick blue solid line indicates the linear absorption due to the E_u phonon mode, data taken from refs. [14,50]. The spectral full-width at half-maximum of the excitation pulses is indicated by the shaded band. **b** Time-resolved measurements of the transient polarization rotation of the probe pulse after excitation with the pump pulses having a polarization of ϕ degrees with respect to the pseudocubic [100] axis at a pump energy of 89 meV. **c** Amplitude of the observed E_g mode excitation (square markers) as extracted by fitting sine functions to the data in **b** and calculated coupling of the excited phonons to the E_g mode (blue circles) vs pump polarization angle ϕ. The errorbars account only for the uncertainty of the fit.

the bandwidth of our excitation pulses and thus these modes cannot be excited in the experiment. To unveil the mechanism of excitation of the E_g mode, we vary the pump photon energy across the phonon absorption band. Figure 3a compares time-resolved transient reflectivity $\Delta R/R$ induced by pumping close to the phonon resonance (85 meV) with off-resonant pumping (124 meV), revealing a striking selectivity of the low-energy mode excitation. The inset in Fig. 3a shows that the amplitude of the excited Raman E_g mode measured for various photon energies increases strongly and peaks at 95 meV close to the absorption peak attributed to the E_u phonon mode centered at 81 meV. Recently, ionic Raman scattering (IRS) or nonlinear phononics was proposed as a mechanism for resonant non-thermal activation of coherent low-energy Raman-active (non-polar) phonon modes upon exciting infrared-active (polar) lattice vibrations[19]. According to this mechanism, the anharmonicity of the lattice potential leads to a nonlinear response when large-amplitude infrared-active ionic vibrations Q_{IR} are excited. The anharmonicity causes a short-living net distortion of the lattice along a Raman coordinate Q_R accompanied by coherent oscillations of the corresponding Raman-active mode around this displaced metastable position. In the general case, the nonlinear coupling can be described by introducing an invariant nonlinear term $\alpha' Q_{IR}^2 Q_R$ in the lattice potential, with α' defining the strength of the coupling and Q corresponding to the normal coordinate of a phonon mode. Despite the strong correlation between the phonon absorption and the E_g mode amplitude, we note that the largest amplitude is observed at a pump photon energy shifted from the peak of the linear phonon absorption. Moreover, the lineshape of the amplitude as a function of the pump photon energy is significantly broader than the linear aborption. These observations indicate that the excitation of the E_g mode is more efficient at the reststrahlen band, where the absorption processes are not dominant and the optical response of the medium is non-dissipative.

To verify and study this nonlinear coupling in the specific case of $LaAlO_3$, we perform a symmetry analysis and density functional theory (DFT) calculations with the ABINIT code[33] to fit a nonlinear phonon-phonon model potential of bulk $R\bar{3}c$ $LaAlO_3$ (see "Methods" and Supplementary Discussion). Although the DFT calculations show that the coupling between the A_{2u} and E_g mode is negligible, they confirm a strong coupling between the E_u and E_g mode. In the case of rhombohedral $LaAlO_3$, containing a high-symmetry three-fold rotation axis along the pseudocubic [111] direction, the IR-active E_u mode has two orthogonal components (E_u^x, E_u^y) oriented in the natural rhombohedral plane (pseudocubic (111)) (see inset Fig. 1a for a schematic including the different orientations). The coupling term is given by $\alpha' = \alpha \cos(2\theta)$, with α a material-dependent constant and θ the angle between the laser polarization projected onto the (111) plane and the x-component of the E_u mode.

In Fig. 3c we show the DFT results for the evolution of the effective coupling coefficient α' with respect to the pump polarization angle ϕ, oriented in the (001) plane, such that $\phi = 0$ corresponds to the pump polarization oriented along the [100] axis. In order to calculate the coupling constant α', the laser polarization in the pseudocubic (001) plane needs to be projected on the (111) plane. As a result α' evolves as a non-trivial periodic function with extrema around $\phi = 0^\circ$ and 112.5°, see Supplementary Discussion. To verify this behavior, we measured the amplitude of the E_g oscillation for the pump polarizations oriented along several pseudocubic crystallographic directions, as shown in Fig. 3b. Figure 3c summarizes the observations, showing a good agreement with predictions of the nonlinear phonon model built from DFT. Together with the dependence on the pump photon energy, this confirms that excitation of the E_g Raman-active mode is governed by the IRS mechanism. Moreover, these selection rules are another strong indication that these lattice dynamics are not driven by the absorption, but are rather non-dissipative relying on the resonant enhancement of the scattering process[19]. The relevance of this mechanism is further corroborated by measurements of the fluence dependence, revealing a linear increase in the E_g mode amplitude[34] (see Supplementary Discussion). These findings are therefore a clear manifestation of the efficient nonlinear phononics mechanism in a wide bandgap insulator in conditions promoting exclusively coherent phonon–phonon coupling. In this sense IRS differs substantially from regular impulsive stimulated Raman scattering in which excitation of coherent phonons is mediated by virtual electronic transitions[34]. Note that the observation of the net structural distortion along the E_g coordinate responsible for the oscillations is not feasible in an all-optical experiment alone and requires use of time-resolved X-ray diffraction[35].

Tunable shear strain

The Fourier analysis (FFT) of the light-induced coherent strain waves as a function of the pump photon energy is summarized in Fig. 4a. We observe that acoustic waves are excited both in the optical transparency window and in the reststrahlen band. The inset of Fig. 4a shows that upon reaching the reststrahlen band, the amplitudes of both strain waves experience a pronounced growth indicating an enhancement at the phonon resonance. The dependence of the strain waves on the pump fluence and

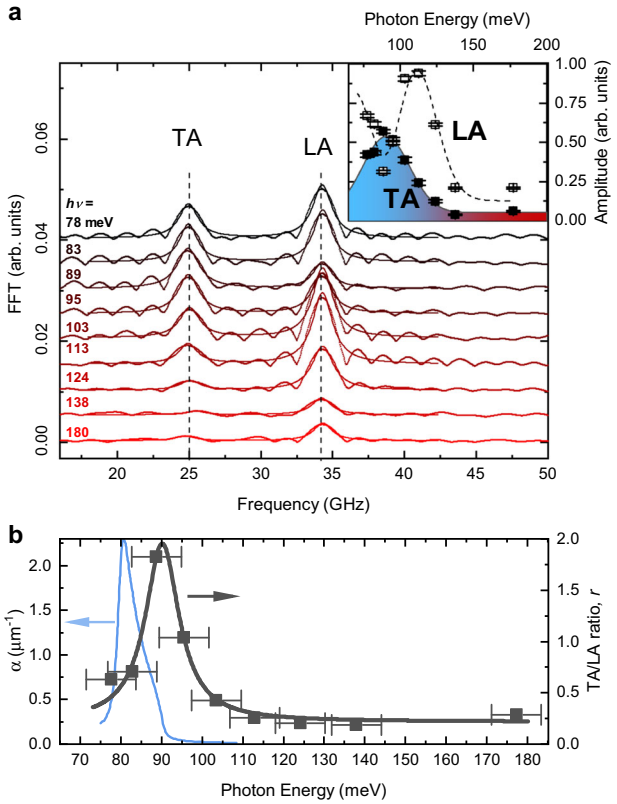

Fig. 4 Tunable shear strain. a Fourier transforms of the measured polarization rotation signals corresponding to strain wave propagation after excitation with different pump energies *hv*. Inset: Pump photon energy dependent amplitude of the two oscillations corresponding to LA and TA strain waves for fixed pump and probe polarizations as obtained from the Fourier transforms shown in panel **a**. The solid and dashed lines are guides to the eyes. The errorbars account for the uncertainty of the fit. **b** Linear absorption due to the infrared-active phonon modes, as taken from ref. [14] (left axis) and ratio *r* of the TA and LA mode amplitudes (right axis) vs photon energy at constant incident fluence. The black line serves as a guide to the eye. The spectral full-width at half-maximum of the excitation pulses is indicated by the errorbars.

polarization are given in Supplementary Note 2. Conventionally, the generation of strain in the transparency window is described by electrostriction[16,36]. In principle, the enhancement of the TA and LA mode amplitudes close to the phonon resonance could simply originate from an increased photon absorption and the anisotropic elastic response of [001] $LaAlO_3$, as this crystal cut is different from the high-symmetry [111] direction, providing a coupling between longitudinal and transverse strain. However, analyzing the strain wave amplitudes, we observe that the presence of the phonon resonance also dramatically renormalizes the ratio *r* between the amplitudes of the TA and LA modes (see Fig. 4b). Our experiments indicate that while their ratio *r* is around 0.2 in the transparency window, it shows a pronounced increase up to 2 in the reststrahlen band. As seen in the inset of Fig. 4a, the renormalization is achieved due to a strong enhancement in the generation of the TA strain wave, which seemingly occurs at the expense of the LA phonon mode. Such an evolution of the ratio with photon energy cannot be explained by direct TA mode excitation via dissipative effects due to an increased photon absorption, especially as the peak of the ratio does not coincide with the phonon absorption peak. Strikingly, the ratio peaks at a higher photon energy, comparable to the position of the maximum amplitude of the E_g mode (see inset Fig. 3a). We propose that this relative and absolute increase in TA mode generation is the result of a phonon-driven enhancement of the coupling between TA and LA modes, in combination with an ionic enhancement of the electrostriction[37]. In the Supplementary Discussion we quantify the elastic constants of $LaAlO_3$ using DFT and show that, out of equilibrium, the distortion along the E_g Raman coordinate driven by the rectification of the phonon field alters the coupling between longitudinal and transverse strain. This change of elastic constants shows that the anisotropic E_g mode can transfer longitudinal strain into shear strain.

Using a combination of time-resolved reflectivity and polarimetry we have studied coherent structural dynamics in $LaAlO_3$ induced by ultrashort excitation of a selected IR-active phonon mode. Our experimental and theoretical analysis uncovers a previously unknown remarkable feature associated with the excitation of the crystal lattice. In addition to the displacement along a Raman coordinate and coherent THz atomic vibrations, expected within a nonlinear lattice excitation regime, we observe an efficient generation of shear strain wave packets. Shear strain following resonant pumping of the crystal lattice in $LaAlO_3$ is likely to be a key element of the metal–insulator transitions, ultrasonic magnetic dynamics, and sonic lattice waves observed in recent years. Importantly, the ratio between the longitudinal and transverse strain waves can be tuned by the pump photon energy in vicinity of the phonon resonance, which hints at a close relation between nonlinear lattice dynamics, coherent lattice symmetry breaking, and (shear) strain generation. Tunable shear strain available on the ultrafast timescales via resonant lattice excitation can be exploited for material control using a wide array of perovskite wide-bandgap anisotropic substrates beyond $LaAlO_3$. Since equilibrium shear strain is an important element for ferroelectric[1], flexoelectric[38], piezoelectric, and magnetoelectric effects, we envision opportunities for ultrafast manipulation of collective excitations in solids. *Note*: A recent complementary work by Neugebauer et al.[39] compares coherent phonons generated by electronic and ionic Raman scattering in $LaAlO_3$.

METHODS

Sample and experimental setup

In our experiments we use commercially available 5 × 5 mm (001) $LaAlO_3$ single crystals with a thickness of 0.5 mm from Crystec GMBH. The mid-infrared pulses (200 fs) are generated in a 0.35-mm-thick GaSe crystal by difference frequency mixing the output of two optical parametric amplifiers (OPAs). The mid-IR pulse is filtered from the OPA output with a germanium filter. The OPAs share the same white light, generated in a sapphire crystal, by the output of a laser amplifier (800 nm, 100 fs, 5 mJ, 1 kHz), which ensures carrier-envelope-phase-stability of the pulses[40]. A small part of the laser output is used to probe the structural dynamics. The transient differential reflectivity ΔR is monitored using a balanced photodetector. The optical birefringence θ_B is tracked using an optical polarization bridge (Wollaston prism) and a balanced photodetector. In both experimental configurations, the probe pulses were focused to a spot with a diameter of 80 µm. The spatial overlap between the pump and probe pulses is obtained by co-propagation of the beams, using an off-axis parabolic mirror, which focuses the pump beam to a spot with a diameter of about 150 µm.

DFT calculations

We simulated the $R\bar{3}c$ phase of $LaAlO_3$ through DFT[41,42] as implemented in the ABINIT package (Ver 8.10.2)[43,44]. We used norm-conserving pseudopotentials[45] to account for the interaction of the nuclei and the electrons. These pseudopotentials were downloaded from the Pseudodojo website[46]. For La we considered 5*s*, 5*p*, 5*d*, 6*s*, and 4*f* as valence states and for Al and O the valence states were considered to be 3*s*, 3*p*, and 2*s*, 2*p*, respectively. We used the PBEsol GGA functional for the exchange correlation interaction[47] and all the calculations were done with a 5 × 5 × 5 mesh of *k*-points for sampling of reciprocal space and a cut-off energy on the plane wave expansion of 45 Hartree. To calculate the phonons, we used density functional perturbation theory as implemented in ABINIT.[48,49]

DATA AVAILABILITY

All data presented in this work are publicly available with identifier (DOI) https://doi.org/10.5281/zenodo.4271722.

CODE AVAILABILITY

The Abinit code is an open source code and is available at https://www.abinit.org.

Received: 8 July 2020; Accepted: 19 November 2020;
Published online: 16 December 2020

REFERENCES

1. Schlom, D. G. et al. Elastic strain engineering of ferroic oxides. *MRS Bull.* **39**, 118–130 (2014).
2. Mundy, J. A. et al. Atomically engineered ferroic layers yield a room-temperature magnetoelectric multiferroic. *Nature* **39**, 523–527 (2016).
3. Haeni, J. et al. Room-temperature ferroelectricity in strained $SrTiO_3$. *Nature* **39**, 758–761 (2004).
4. Schlom, D. G. et al. Strain tuning of ferroelectric thin films. *Annu. Rev. Mater. Res.* **39**, 589–626 (2007).
5. Sando, D. et al. Crafting the magnonic and spintronic response of $BiFeO_3$ films by epitaxial strain. *Nat. Mater.* **39**, 641–646 (2013).
6. Wen, H. et al. Electronic origin of ultrafast photoinduced strain in $BiFeO_3$. *Phys. Rev. Lett.* **39**, 037601 (2013).
7. Lejman, M. et al. Giant ultrafast photo-induced shear strain in ferroelectric $BiFeO_3$. *Nat. Commun.* **39**, 1–7 (2014).
8. Afanasiev, D. et al. Laser excitation of lattice-driven anharmonic magnetization dynamics in dielectric $FeBO_3$. *Phys. Rev. Lett.* **39**, 147403 (2014).
9. Baldini, E. et al. Exciton control in a room temperature bulk semiconductor with coherent strain pulses. *Sci. Adv.* **39**, eaax2937 (2019).
10. Demenev, A. A. et al. Ultrafast strain-induced switching of a bistable cavity-polariton system. *Phys. Rev. B* **39**, 100301 (2019).
11. Kuznetsov, A. S., Biermann, K. & Santos, P. V. Dynamic acousto-optical control of confined polariton condensates: from single traps to coupled lattices. *Phys. Rev. Res.* **39**, 023030 (2019).
12. Sie, E. J. et al. An ultrafast symmetry switch in a Weyl semimetal. *Nature* **39**, 61–66 (2019).
13. Zhang, M. Y. et al. Light-induced subpicosecond lattice symmetry switch in $MoTe_2$. *Phys. Rev. X* **39**, 021036 (2019).
14. Caviglia, A. D. et al. Ultrafast strain engineering in complex oxide heterostructures. *Phys. Rev. Lett.* **39**, 136801 (2012).
15. Mogunov, I. A. et al. Ultrafast insulator-metal transition in VO_2 nanostructures assisted by picosecond strain pulses. *Phys. Rev. Appl.* **39**, 14054 (2019).
16. Ruello, P. & Gusev, V. E. Physical mechanisms of coherent acoustic phonons generation by ultrafast laser action. *Ultrasonics* **39**, 21–35 (2015).
17. Först, M. et al. Spatially resolved ultrafast magnetic dynamics initiated at a complex oxide heterointerface. *Nat. Mater.* **39**, 883–888 (2015).
18. Först, M. et al. Multiple supersonic phase fronts launched at a complex-oxide heterointerface. *Phys. Rev. Lett.* **39**, 027401 (2017).
19. Först, M. et al. Nonlinear phononics as an ultrafast route to lattice control. *Nat. Phys.* **39**, 854–856 (2011).
20. Wordenweber, R. W. Growth of high-T_c thin films. *Supercond. Sci. Technol.* **39**, 79339–79344 (1999).
21. Prellier, W., Lecoeur, P. & Mercey, B. Colossal-magnetoresistive manganite thin films. *J. Phys. Condens. Matter* **39**, 915–944 (2001).
22. Middey, S., Chakhalian, J., Mahadevan, P., Freeland, J. & Millis, A. et al. Physics of ultrathin films and heterostructures of rare-earth nickelates. *Annu. Rev. Mater. Res.* **39**, 305–334 (2016).
23. Zhang, Z. M., Choi, B. I., Flik, M. I. & Anderson, A. C. Infrared refractive indices of $LaAlO_3$, $LaGaO_3$, and $NdGaO_3$. *J. Opt. Soc. Am. B* **39**, 2252–2257 (1994).
24. Abrashev, M. V. et al. Comparative study of optical phonons in the rhombohedrally distorted perovskites $LaAlO_3$ and $LaMnO_3$. *Phys. Rev. B* **39**, 4146–4153 (1999).
25. Fredrickson, K. D., Lin, C., Zollner, S. & Demkov, A. A. Theoretical study of negative optical mode splitting in. *Phys. Rev. B* **39**, 134301 (2016).
26. Lim, S. G. et al. Dielectric functions and optical bandgaps of high-K dielectrics for metal-oxide-semiconductor field-effect transistors by far ultraviolet spectroscopic ellipsometry. *J. Appl. Phys.* **39**, 4500–4505 (2002).
27. Chernova, E. et al. Optical NIR-VIS-VUV constants of advanced substrates for thin-film devices. *Opt. Mater. Express* **39**, 3844–3862 (2017).
28. Scott, J. F. Raman study of trigonal-cubic phase transitions in rare-earth aluminates. *Phys. Rev.* **39**, 823–825 (1969).
29. Matsuda, O., Wright, O. B., Hurley, D. H., Gusev, V. E. & Shimizu, K. Coherent shear phonon generation and detection with ultrashort optical pulses. *Phys. Rev. Lett.* **39**, 095501 (2004).
30. Carpenter, M.A., Sinogeikin, S.V., Bass, J.D., Lakshtanov, D.L. & Jacobsen, S.D. Elastic relaxations associated with the $Pm\bar{3}$ m-$R\bar{3}c$ transition in $LaAlO_3$: I. Single crystal elastic moduli at room temperature. *J. Condens. Matter. Phys.* **22**, 035403 (2010).
31. Babilotte, P. et al. Femtosecond laser generation and detection of high-frequency acoustic phonons in gaas semiconductors. *Phys. Rev. B* **39**, 245207 (2010).
32. Cancellieri, C. et al. Electrostriction at the $LaAlO_3$ /$SrTiO_3$ interface. *Phys. Rev. Lett.* **39**, 056102 (2011).
33. Gonze, X. et al. The Abinitproject: Impact, environment and recent developments. *Comput. Phys. Commun.* **39**, 107042 (2020).
34. Yan, Y.-X., Gamble Jr, E. B. & Nelson, K. A. Impulsive stimulated scattering: general importance in femtosecond laser pulse interactions with matter, and spectroscopic applications. *J. Chem. Phys.* **39**, 5391–5399 (1985).
35. Först, M. et al. Displacive lattice excitation through nonlinear phononics viewed by femtosecond x-ray diffraction. *Solid State Commun.* **39**, 24–27 (2013).
36. Gusev, V., Picart, P., Mounier, D. & Breteau, J. M. On the possibility of ultrashort shear acoustic pulse excitation due to the laser-induced electrostrictive effect. *Opt. Commun.* **39**, 229–236 (2002).
37. Nova, T. F., Disa, A. S., Fechner, M. & Cavalleri, A. Metastable ferroelectricity in optically strained SrTiO3. *Science* **39**, 1075–1079 (2019).
38. Zubko, P., Catalan, G. & Tagantsev, A. K. Flexoelectric effect in solids. *Annu. Rev. Mater. Res.* **39**, 387–421 (2013).
39. Neugebauer, M. J. et al. Comparison of coherent phonon generation by electronic and ionic raman scattering in $LaAlO_3$. Preprint at https://arxiv.org/abs/2010.12943 (2020).
40. Sell, A., Leitenstorfer, A. & Huber, R. Phase-locked generation and field-resolved detection of widely tunable terahertz pulses with amplitudes exceeding 100 MV/cm. *Opt. Lett.* **39**, 2767–2769 (2008).
41. Hohenberg, P. & Kohn, W. Inhomogeneous electron gas. *Phys. Rev.* **39**, B864 (1964).
42. Kohn, W. & Sham, L. J. Self-consistent equations including exchange and correlation effects. *Phys. Rev.* **39**, A1133 (1965).
43. Gonze, X. et al. First-principles computation of material properties: the ABINIT software project. *Comput. Mater. Sci.* **39**, 478–492 (2002).
44. Torrent, M., Jollet, F., Bottin, F., Zerah, G. & Gonze, X. Implementation of the projector augmented-wave method in the ABINIT code: application to the study of iron under pressure. *Comput. Mater. Sci.* **39**, 337–351 (2008).
45. Hamann, D. R. Optimized norm-conserving Vanderbilt pseudopotentials. *Phys. Rev. B* **39**, 085117 (2013).
46. van Setten, M. et al. The pseudodojo: training and grading a 85 element optimized norm-conserving pseudopotential table. *Comput. Phys. Commun.* **39**, 39–54 (2018).
47. Perdew, J. P. et al. Restoring the density-gradient expansion for exchange in solids and surfaces. *Phys. Rev. Lett.* **39**, 136406 (2008).
48. Gonze, X. & Lee, C. Dynamical matrices, born effective charges, dielectric permittivity tensors, and interatomic force constants from density-functional perturbation theory. *Phys. Rev. B* **39**, 10355–10368 (1997).
49. Gonze, X. First-principles responses of solids to atomic displacements and homogeneous electric fields: implementation of a conjugate-gradient algorithm. *Phys. Rev. B* **39**, 10337–10354 (1997).
50. Willett-Gies, T., DeLong, E. & Zollner, S. Vibrational properties of bulk $LaAlO_3$ from Fourier-transform infrared ellipsometry. *Thin Solid Films* **39**, 620–624 (2014).

ACKNOWLEDGEMENTS

The authors thank T.C. van Thiel for fruitful discussions and G. Koster for providing an $LaAlO_3$ sample. This work was partially supported by The Netherlands Organization for Scientific Research (NWO/OCW) as part of the VIDI program, by the EU through the European Research Council, grant No. 677458 (AlterMateria). E.B. and A.S. acknowledge the FRS-FNRS, the Consortium des Equipements de Calcul Intensif (CÉCI, grants No. 2.5020.11 and No. 1175545), and Tier-1 supercomputer of the Fédération Wallonie-Bruxelles funded by the Walloon Region (Grant No. 1117545).

AUTHOR CONTRIBUTIONS

A.D.C. conceived the project. J.R.H. and D.A. carried out the experiments and analyzed the data. A.S. and E.B. performed the DFT calculations. All authors discussed the results. The manuscript was written by J.R.H., D.A., and A.D.C. with feedback and input from the coauthors.

COMPETING INTERESTS

The authors declare no competing interests.

ADDITIONAL INFORMATION

Supplementary information is available for this paper at https://doi.org/10.1038/s41535-020-00297-z.

Correspondence and requests for materials should be addressed to J.R.H. or A.D.C.

Reprints and permission information is available at http://www.nature.com/reprints

Publisher's note Springer Nature remains neutral with regard to jurisdictional claims in published maps and institutional affiliations.